Ultra-sensitive Ebola virus antigen sensing via three-dimensional nanoantenna arrays

*Faheng Zang, Zhijuan Su, Liangcheng Zhou, Krishnamurthy Konduru, Gerardo Kaplan and Stephen Y. Chou**

Dr. Faheng Zang, Dr. Zhijuan Su, Dr. Liangcheng Zhou, and Prof. Stephen Y. Chou
Department of Electrical Engineering, Princeton University, Princeton, NJ 08544, USA
E-mail: Stephen Y. Chou (chou@princeton.edu)

Dr. Krishnamurthy Konduru and Dr. Gerardo Kaplan
Laboratory of Emerging Pathogens, Center for Biologics Evaluation and Research, Food and Drug Administration, Silver Spring, MD 20993, USA

Keywords: nanoantenna, optical resonance, fluorescence enhancement, biosensors, Ebola virus glycoprotein

Abstract: Sensitive detection of pathogens is crucial for early disease diagnosis and quarantine, which is of tremendous need in controlling severe and fatal illness epidemic such as Ebola virus (EBOV) disease. Serology assays can detect EBOV-specific antigens and antibodies cost-effectively without sophisticated equipment; however, they are less sensitive than reverse transcriptase polymerase chain reaction (RT-PCR) tests. In this paper, a three-dimensional plasmonic nanoantenna assay sensor is developed as an on-chip immunoassay platform for ultra-sensitive detection of Ebola virus (EBOV) antigens. The EBOV sensor exhibits substantial fluorescence intensity enhancement in immunoassays compared to flat gold substrate. The nanoantenna-based biosensor successfully detects EBOV soluble glycoprotein (sGP) in human plasma down to 220 fg/mL, a significant 240,000-fold sensitivity improvement compared to the 53 ng/mL EBOV antigen detection limit of the existing rapid EBOV immunoassay. In a mock clinical trial, the sensor detects sGP-spiked human plasma samples at two-times the limit of detection with 95.8% sensitivity. The results combined have highlighted the nanosensor's extraordinary capability of detecting EBOV antigen at ultra-low concentration compared to

existing immunoassay methods. It is a promising next-generation bioassay platform for early-stage disease diagnosis and pathogen detection for both public health and national security applications.

Infection with Ebola virus (EBOV), a *Filoviridae* classified as a "Category A" bioterrorism agent, results in high mortality rates in humans and poses a significant threat to the public health and national safety worldwide[1]. The recent 2013-2016 EBOV epidemic and current 2018-2019 outbreak in West Africa underscored the need to develop highly sensitive test to diagnose infection as early as possible, which is essential for treatment and quarantine purposes[2]. Unfortunately, there are currently no US Food and Drug Administration (FDA) licensed vaccines or approved treatments against EBOV infection, and supportive therapy is mainly used to treat patients. Reverse transcriptase polymerase chain reaction (RT-PCR) is an effective tool to diagnose EBOV infection[3]. RT-PCR is currently used in central facilities where a controlled environment is required to prevent contaminations during the process and precisely programed temperature cycles are utilized to amplify the extracted target DNA fragment[4]. Immunoassays targeting at EBOV antigen proteins have been explored and developed for EBOV infection as an alternative and complementary diagnostic tool to RT-PCR; however, due to relatively low sensitivity, the immunoassays are mainly being utilized for general EBOV disease screening and post-epidemic surveys. The FDA has granted Emergency Use Authorization (EUA) to EBOV rapid antigen tests based on the detection of the viral protein VP40. OraQuick® Ebola Rapid Antigen Test currently holds EUA status but has a low sensitivity (limit of detection, LoD) of 53 ng/mL of VP40 in blood and 7.6 ng/mL in oral fluid, and it is unclear whether this test can be used for early detection of EBOV infection compared to RT-PCR. There are also a few alternative EBOV antigens and antibodies assays which are currently in research phase. These include an antibody gold nanoparticle-based lateral flow colorimetric immunoassay[5] (LoD of 200 ng/mL EBOV antigen)

and an antigen field-effect transistor[6] (LoD of 1ng/mL EBOV antigen), but these tests also show lower sensitivity compared to RT-PCR. Therefore, there is an urgent need to advance highly sensitive EBOV immunoassay for early antigen quantification and disease diagnosis.

Nanomaterials and nanodevices have shown promising features as transducing elements in biosensor system owing to their enhanced interaction with biological reagents at nanoscale[7]. Plasmonic nanostructures in particular are attracting increased attention in biosensing applications because of their high sensitivity to detect changes on sensor surfaces[8]. However, development of plasmonic biosensors with high specificity, cost-effective fabrication, and integration with existing bioassay is still challenging [9]. We focused our strategy on nanostructured photonic devices as ultrasensitive transducers to allow high sensitivity detection of EBOV antigens. Previously, our team developed nanoimprint lithography (NIL) process to enable fabrication of three-dimensional nanostructures on a large scale[10]. Here, we develop a three-dimensional nanoscale antenna array and leverage the optical resonance feature to enhance the fluorescence signal level and tune it for EBOV antigen early diagnosis, and pixelated fluorescence hotspot analysis for low concentration EBOV antigen sensing. We utilize this nanoantenna array-based biosensing platform to select the best capture and detection antibody pair for an EBOV glycoprotein antigen sandwich assay. This sensor system improved more than 240,000-fold the EBOV antigen detection sensitivity compared to existing FDA-recommended immunoassay-based test, and 4500-fold compared to the best EBOV biosensors in the research phase. Meanwhile, the nanoantenna platform is fabricated through scalable nanoimprint processes, and has demonstrated excellent compatibility with the industrial standard 96-well plate and sandwich assay format. Therefore, the nanoantenna sensor platform has tremendous potentials to be implemented as a universal ultrasensitive immunoassay platform to diagnose a wide arrange of diseases.

The nanoantenna array sensor platform comprises a thin layer of plasmonic nanoantenna array with its surface linked with, through a molecular linker layer, EBOV capture agents (**Figure 1a**). The nanoantenna array consists of silicon-dioxide nanopillar array with an Au nanodisk on top of each pillar, Au nanodots on the pillar sidewall, and Au backplane at the foot of pillars. The disks and planes form a plasmonic nanocavity array, maximize the excitation laser absorbance and improve light emissions from bound fluorescence labels. The nanodots in the nanocavity can further enhance positioning of fluorophores in the high field areas, and thus drastically increase the fluorescence signal emission from the molecules.

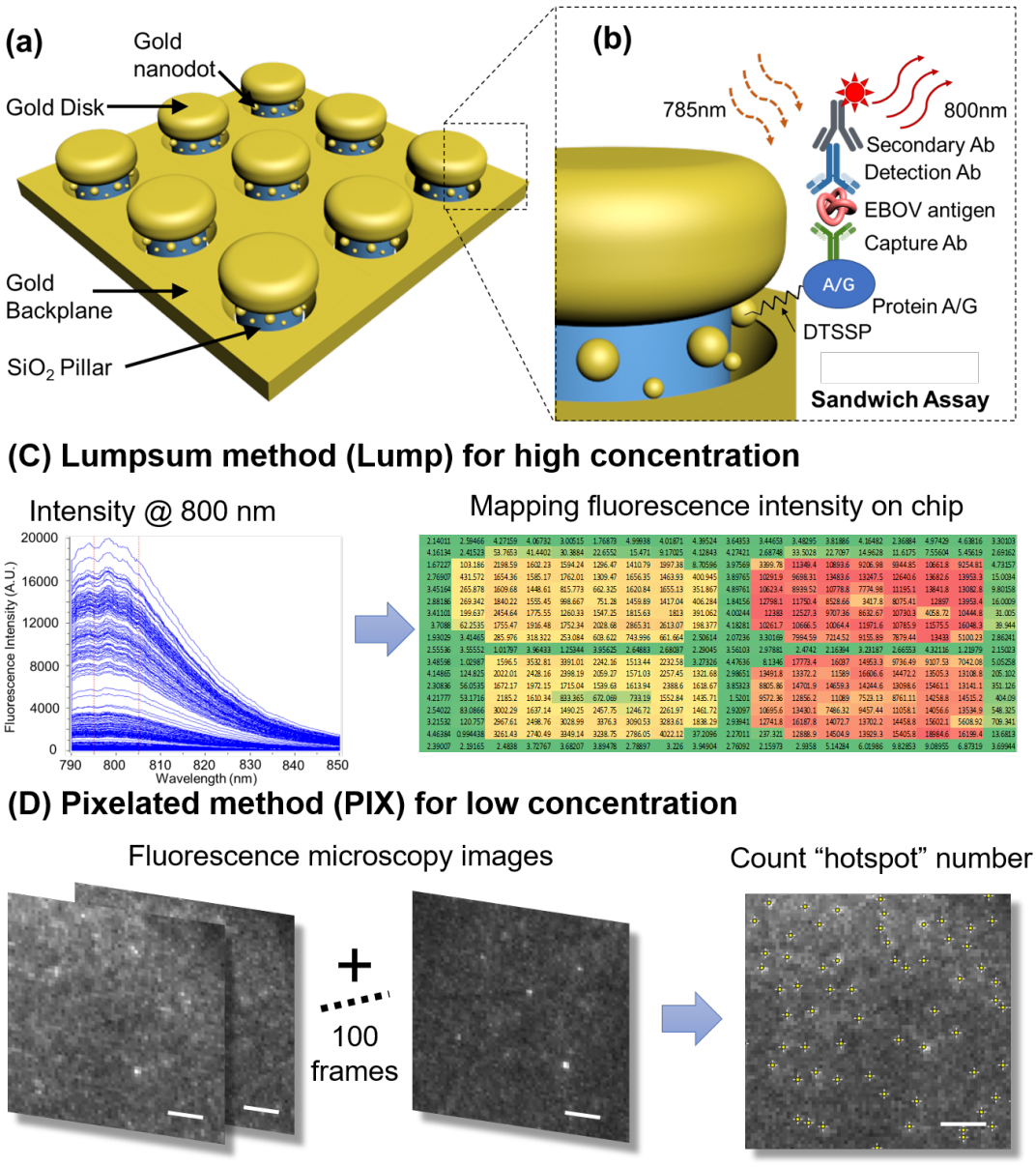

Figure 1. The EBOV sensor nanostructures and fluorescence sensing methods. (a) Schematic of nanoantenna array. (b) Exploded view showing the details of single nanopillar structures and a sample EBOV sandwich assay structure on-chip. (c) Lumpsum (LUMP) method for counting overall fluorescence intensity at high antigen concentration. (d) Pixelated (PIX) method for low antigen concentration analysis by fluorescence hotspot counting (scale bars represent 10µm).

Figure 1a shows the schematic of the nanoantenna array structure. The gold nano disks and backplane are separated by silicon dioxide pillars, forming nanocavities that can efficiently absorb

laser irradiation at the nanoantenna's resonance wavelength. Tiny gold nanoparticles are present on the SiO_2 pillar surfaces where the localized electromagnetic field are the highest around the nanostructures. The exploded view in Figure 1(b) demonstrated the conceptual format of EBOV sandwich assay on the nanoantenna array platform. Before starting assay, the sensor surfaces were first functionalized with a self-assembled monolayer (SAM) of 3,3'-dithiobis (sulfosuccinimidyl propionate) (DTSSP) to create thiol-gold link, and subsequently bound a layer of Protein A/G as antibody anchors (see **Experimental Sections** for details). The SAM layer of DTSSP plus the Protein A/G layer also serves as a spacer with the thickness of around 6.1 nm to prevent irradiative fluorescence signal loss on the gold surfaces. An Fc fusion of the extracellular domain of EBOV glycoprotein (GP)[11] (EBOVgp-Fc) and EBOV soluble glycoprotein (sGP) were studied as antigens in the sandwich assay. Proteins translated from the EBOV GP gene that share the N-terminus amino acid sequence are detailed in **Electronic Supporting Information (ESI)**. A rabbit IgG polyclonal antibody raised against a conserved peptide corresponding to the N-terminus of the EBOV GP[12] and a mouse IgG monoclonal antibody were used as EBOV antigen-specific capture and detection antibodies, respectively. An IRDye800 infrared fluorophore-labeled goat anti-mouse IgG secondary antibody (785nm peak excitation, 800nm peak emission) was added before the end of the assay (see Experimental section for detailed assay protocols). Fluorescence microscopy imaging and spectrum analysis were utilized to quantitatively study the EBOV antigen binding on the nanoantenna array sensor surfaces are the assay. We use a Lumpsum (LUMP) and Pixelated (PIX) to quantify fluorescence activities on the sensor at high and low antigen concentrations, respectively. The LUMP method surveys a large on-chip area and measures areal fluorescence intensity. When the antigen concentration is ultra-low, the PIX method counts separated and dispersed fluorescence "hot-spot" numbers with "flickering" behaviors in continuous 100 picture

frames over 10 seconds. The fluorophore flickering effects have been previously studied as an effective methods to reliably quantify single-molecule fluorophore flicking on a nanoantenna or plasmonic-enhanced structures[10c, 13]. The detailed configurations of LUMP and PIX methods are described in **Experimental Sections**.

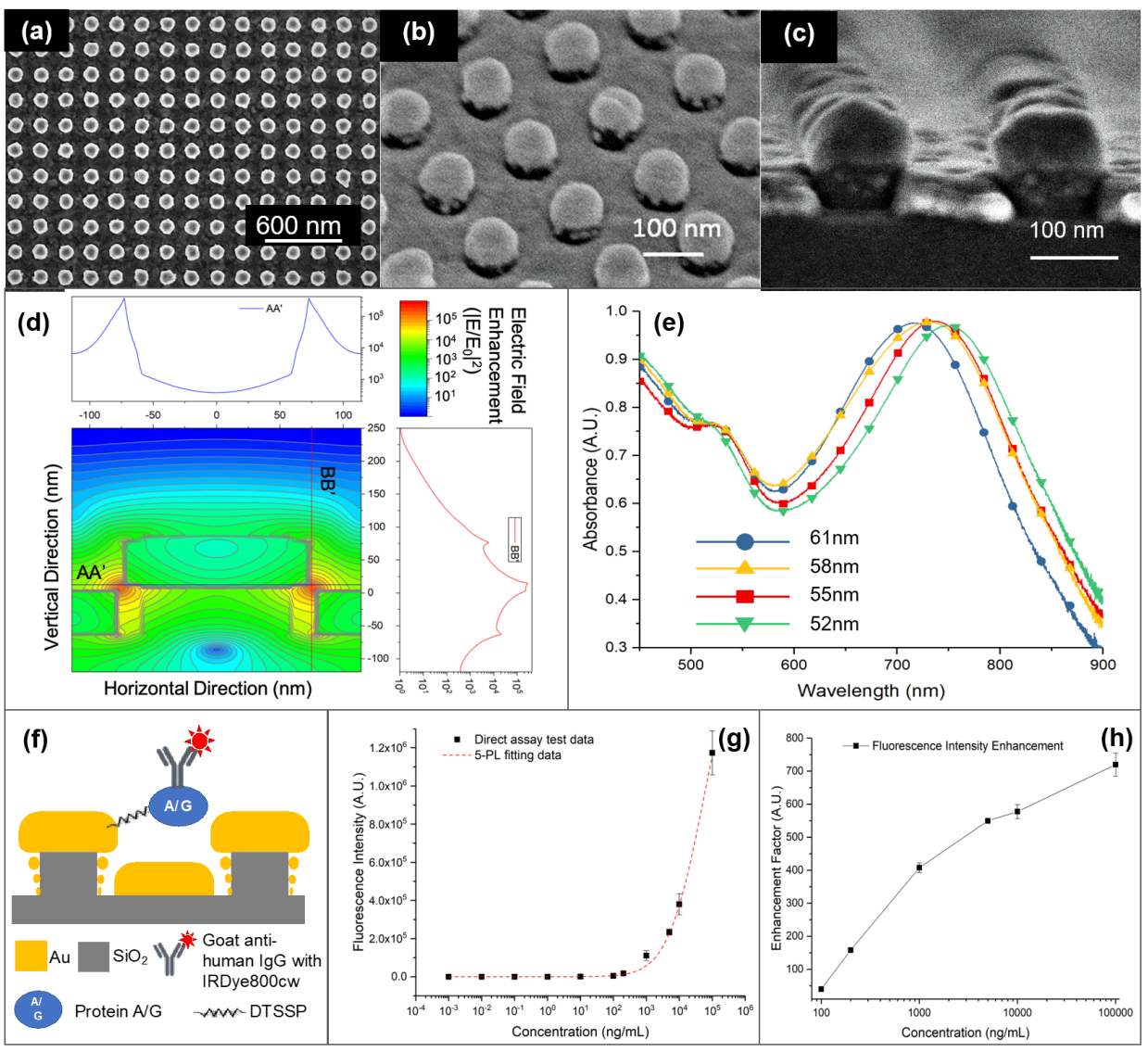

Figure 2. Characterization of the nanoantenna array EBOV sensor after nanofabrication. (a) Scanning electron microscopy (SEM) image showing the top-down view of the nanoantenna array after nanofabrication processes on a 4-inch wafer; (b) a prospect view SEM image showing the Au nano disks

on SiO_2 pillars; (c) SEM image showing discrete distribution of gold nanoparticles on the nanoantenna array SiO_2 nanopillar sidewalls. (d) FDTD simulation of the electrical field enhancement ($|E/E_0|^2$) in a nanoantenna unit. (e) Absorption spectra of the nanoantenna array with different nanopillar heights (52nm – 61nm). (f) Schematic of antibody direct binding assay on the nanoantenna array biosensor. (g) Antibody direct binding assay standard curve. (i) Fluorescence intensity enhancement on the nanoantenna array compared to flat gold surfaces after antibody binding assay. (N=27, error bars stand for standard deviations)

Figure 2a, 2b, and 2c are scanning electron microscopy images of the nanoantenna array geometries after nanofabrication. We have successfully fabricated the nanoantenna array EBOV biosensor on a 4-inch wafer with high fidelity using nanoimprint lithography (NIL) processes. The nanostructures on our sensor are featured by a periodic SiO_2 dielectric pillar array (200 nm pitch and ~100 nm diameter), a Ti/Au (1.5 nm/50 nm thick) disk (~135 nm diameter) on top of each pillar, and a gold backplane on the foot of the pillars (Figure 2a). In addition, gold nanodots with less than 10nm in diameter are randomly located on the SiO_2 nanopillar walls (Figure 2b, c). The metallic disk and backplane form a 3D cavity antenna unit which is very effective in absorbing incoming light from far field and amplifying light generated in the near field.

FDTD simulation was performed to study the theoretical source of fluorescence enhancement from the nanoantenna. The simulation focused on both excitation enhancement (electric field enhancement) and fluorophore emission quantum efficiency improvement. Figure 2d shows the normalized electric field enhancement ($|E/E_0|^2$) at the nanoantenna cross-section. The field enhancement value is normalized against the lowest the field enhancement location of 250 nm above the gold backplane. It is shown that the strongest field enhancement location is in between the gold top disk and backplane. This space also includes the narrow cavity between the SiO_2 pillar and the gold backplane, and the field enhancement ($|E/E_0|^2$) goes up to 10^5 order. At the edge of gold top disk, the field enhancement is around 10^4. With the fluorophore location at 6.1 nm – 35.4

nm above gold surfaces, the average electric field enhancement is 11350. A similar FDTD simulation resulted in an average field enhancement factor of 87 for the same distance of 6.1 nm – 35.4 nm above gold surface. Therefore, the analytical excitation enhancement f_E of the nanoantenna compared to a flat gold surface is 130 folds. The fluorophore used in this work has an intrinsic quantum efficiency of η=7% [10c, 14]. The radiative factor is defined as the ratio of radiated power (P_r) over the total radiated power of a dipole without nanoantenna (P_0), and non-radiative factor is defined as the ratio of non-radiative power loss (P_{nr}) over P_0. At 800 nm wavelength, the radiative factor $f_r \equiv P_r/P_0$= 33.3, the non-radiative factor $f_{nr} \equiv P_{nr}/P_0$=21.4. The enhancement of the quantum efficiency is then $f_\eta = f_r /[(1- \eta)+ \eta (f_r + f_{nr})]$=7. It should be noted that, if a fluorophore with higher intrinsic quantum efficiency were used, the enhancement from emission will degraded. Therefore, the overall analytical fluorescence enhancement of a single fluorophore is strongly determined by the electric field enhancement from the nanoantenna. The analytical total enhancement is $f_F = f_E f_\eta$= 910. The experimental fluorescence enhancement factor is measured to be 720 at 100 μg/mL antibody concentration (Figure 2i). The experimental enhancement factor is expected to be lower than the analytical result due to (1) the rounded corners on the top-disk and backplane of a nanoantenna after nanofabrication compared to the shape corners in the simulation model, and (2) the under-saturated fluorophore density compared to the conformal fluorophore coverage assumption in the simulation. The experimental fluorescence enhancement factor is on the similar scale compared to other nanoantenna works[13].

The optical absorption property of the nanoantenna array sensor was studied experimentally using a Hiroba Raman spectrometer with a white light source. Figure 2e shows that the nanoantenna array nanostructures can efficiently absorb light at the resonance wavelength of 700 nm with over 95% light absorption efficiency. The resonance peak can blue-shift for over 50 nm

in wavelength through increasing the SiO_2 pillar height from 52 nm to 61 nm, validating the optical tunability of the nanoantenna array through nanofabrication.

An antibody direct binding assay test was first performed to validate the fluorescence enhancement performance of the nanoantenna array sensor (Figure 2f). We utilized IRDye-800cw fluorophore-labeled goat anti-human IgG at various concentration to characterize the fluorescence enhancement from the nanoantenna array. We also performed the same assay protocol on flat gold and SiO_2 surface as control experiments. Figure 2g shows the sensor response to increasing antibody concentrations in the direct binding assay. The fluorescence enhancement factor (EF) is the ratio of fluorescence intensity at 800 nm from the nanoantenna array surface over that from a conventional flat substrate under the same assay conditions. A detailed description of EF measurement is **Experimental Sections**. Figure 2h shows EF of the nanoantenna array compared to flat gold substrate. In both experiments involves nanoantenna and flat gold, a SAM layer and Protein A/G have served as a spacer to prevent significant irradiative loss close to gold. The EF maximized at 720 with 100 μg/mL antibody concentration. The increasing EF with antibody concentration may resulted from accumulation of more fluorophores in the cavities of the nanoantenna where high electric field is located especially in the presence of the drying process before imaging. This is a direct validation of the nanoantenna array fluorescence signal enhancement compared to conventional flat assay substrates, validating the great potential, and have validated the suitability of using the nanoantenna array in bioassay.

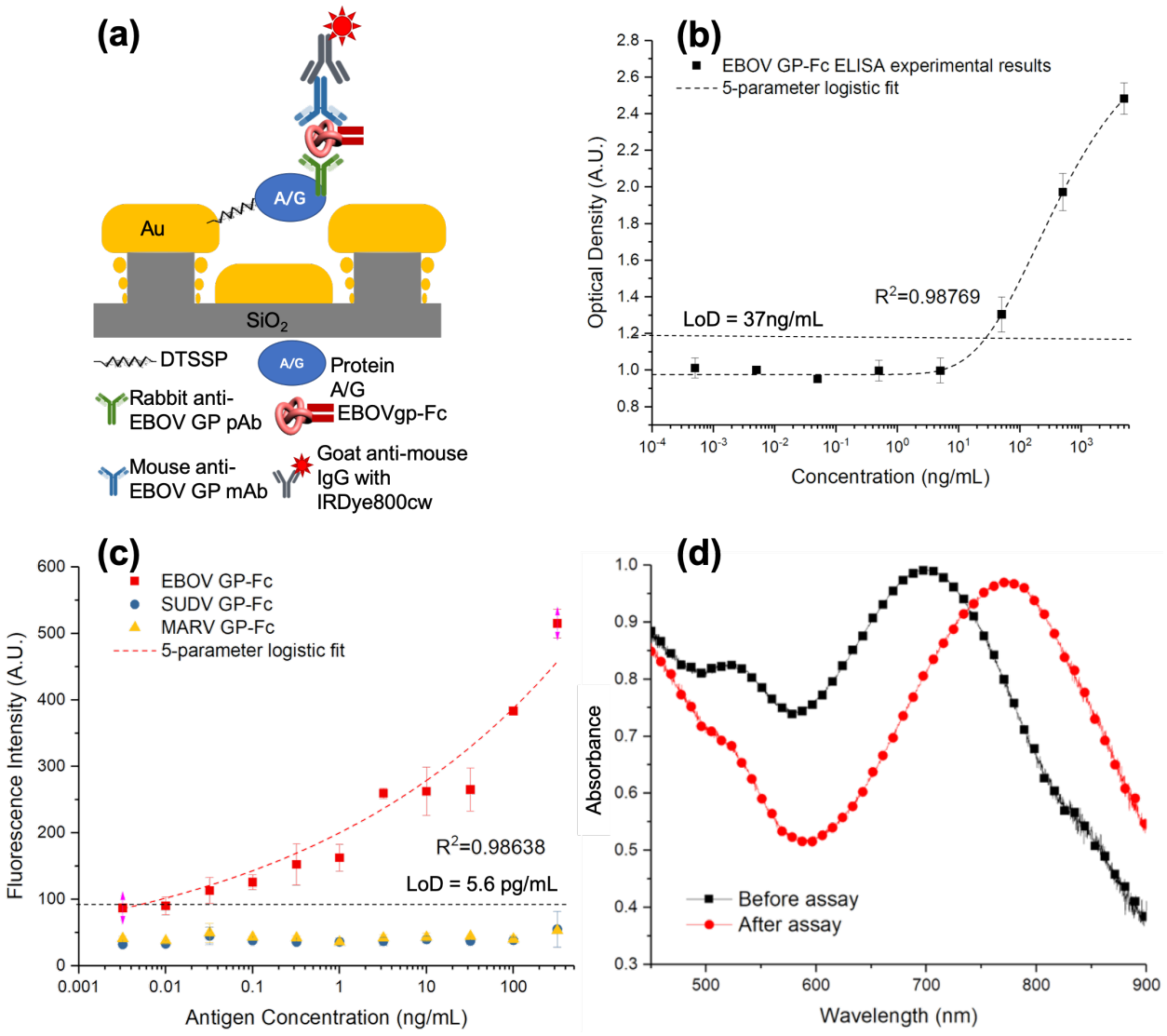

Figure 3. EBOVgp-Fc-spiked PBS buffer bioassay test. (a) Sandwich assay format for EBOVgp-Fc detection using the nanoantenna array biosensor. (b) Bioassay responses to increasing EBOVgp-Fc antigen concentration in ELISA. (N=27, error bars stand for standard deviations) (c) Sandwich assay responses to increasing EBOVgp-Fc antigen concentration using the nanoantenna array. (N=27, error bars stand for standard deviations) (d) the nanoantenna array absorbance characteristics change before and after sandwich assay against EBOVgp-Fc at 320 ng/mL.

Ebola antigens – EBOV sGP and EBOVgp-Fc –were detected using the nanoantenna array biosensor platform through a sandwich assay protocol. **Figure 3a** shows a schematic representation of the EBOV sandwich bound (protein A/G-cAB-antigen-dAb-secondary antibody)

to the nanoantenna array structure. Detailed sandwich assay protocols are detailed in Experimental Section. Laser excitation at 785nm (10mW/cm^2) resulted in IR light emission signal at around 800nm. We performed side-by-side comparison between our proposed the nanoantenna array-based sandwich assay and ELISA using the same antibodies and antigens (see the modified ELISA protocol in Experimental Section).

Figure 3b shows a dose-dependent correlation between optical density (OD) and EBOVgp-Fc target molecule concentrations by ELISA. While there is a linearly-relationship at higher EBOVgp-Fc concentrations, there is no specific signal at concentrations below 10 ng/mL. The limit of detection (LoD) of EBOVgp-Fc by ELISA was determined as 37 ng/mL using five-parameter logistic fitting method and three times of standard deviation from background. In comparison, the nanoantenna array sensing platform reduced the LoD of EBOVgp-Fc to 5.6 pg/mL using LUMP method (Figure 3c). To determine the specificity of EBOV GP test in the nanoantenna array platform, we used two negative control antigens, the Fc fusion proteins of the MARV GP (MARVgp-Fc) and SUDV GP (SUDVgp-Fc) which share similar biomolecular structures with EBOVgp-Fc. The cAb-dAb pair of antibodies did not react with the glycoprotein of Sudan virus (SUDV), a filovirus belonging to the same genus than EBOV (Ebola virus), and Marburg virus (MARV), a filovirus that belongs to a different genus (Marburg virus), indicating that the assay was specific for EBOV. Furthermore, omission of any of the components of the antigen-antibody sandwich resulted in minimal background-level signal in both the nanoantenna array and ELISA formats of the test. The nanoantenna array sensor showed good dynamic responses to EBOVgp-Fc with over 5 magnitudes of dynamic range from 3.2 pg/mL to 320 ng/mL with a fluorescence signal level ranged from below 100 to over 500 arbitrary units (A.U.). In contrast, the fluorescence intensities from the negative controls were below 50 A.U. for the entire antigen concentration

range (3.2 pg/mL – 320 ng/mL). Additional images from PIX method on EBOVgp-Fc tests are available as **Figure S1** in the **ESI**. These results validate the excellent sensitivity and specificity of the nanoantenna array-based EBOV assay. The optical properties of the nanoantenna array have been studied. The nanoantenna array resonance wavelength in the absorbance spectrum red-shifted from 700 nm to 785 nm at the antigen concentration of 320 ng/mL (Figure 3d), matching laser excitation wavelength for maximized laser energy absorption. The results above have shown the nanoantenna array as a suitable sandwich immunoassay platform in EBOV antigen test. The nanoantenna array has shown significant enhancement in EBOV detection sensitivity compared to conventional ELISA methods. The nanoantenna array-based EBOV antigen assay also achieved high specificity owing to the combination of highly specific capture-detection antibody pair and a sandwich assay format.

While the nanoantenna array-sensor response to EBOVgp-Fc in buffer media validates its sensitivity and selectivity, direct detection of EBOV soluble glycoprotein (EBOV sGP) in clinically relevant samples can provide more valuable information of the sensor performance in real-life. Here, we performed the nanoantenna array assay test in EBOV sGP-spiked human plasma samples. The original EBOV sGP stock sample was kept in serum-free OptiMEM medium at a concentration of approximately 120 ng/mL as estimated by ELISA using purified EBOVgp-Fc as the antigen standard.

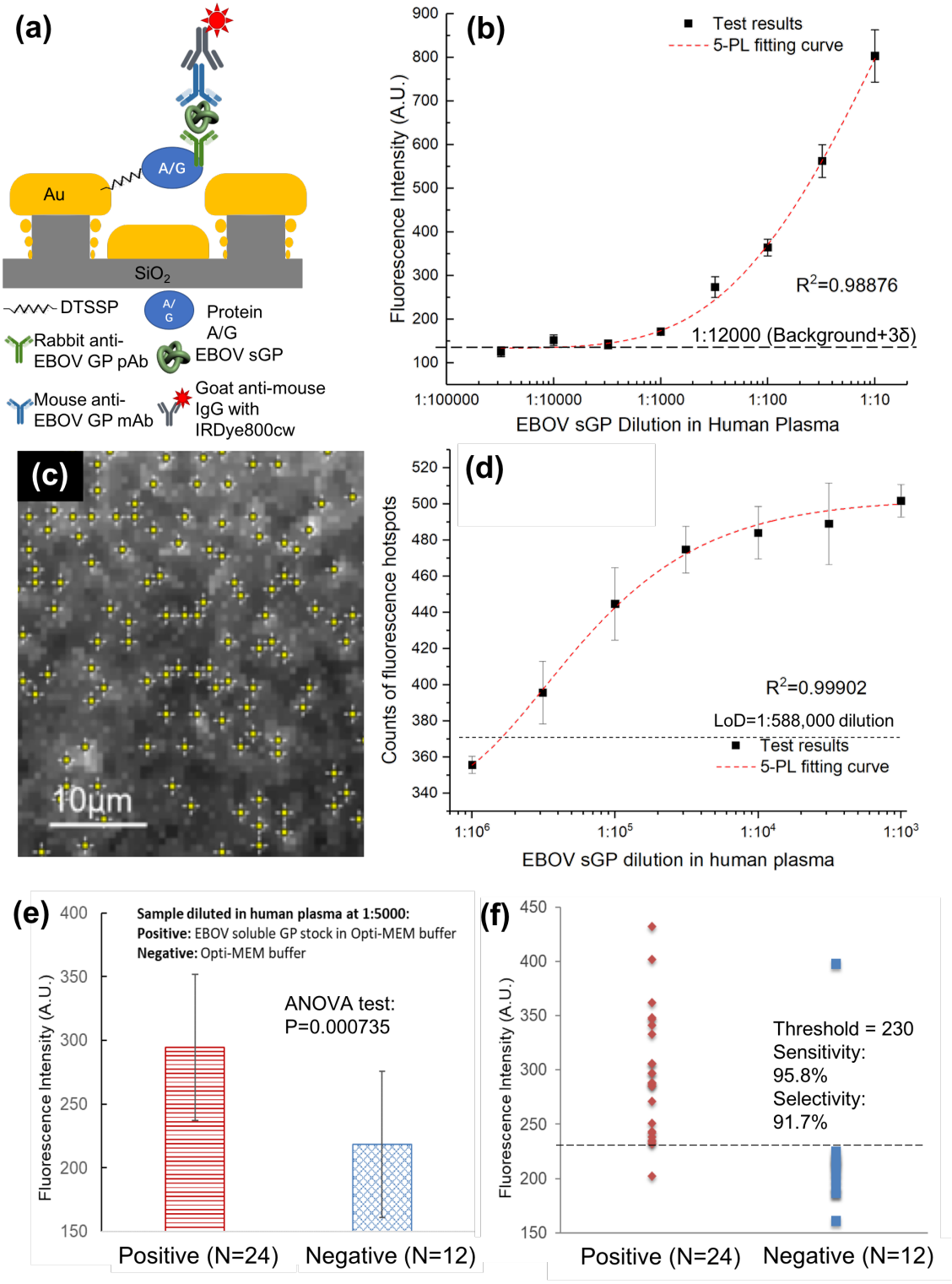

Figure 4. EBOV sGP-spiked human plasma study using the nanoantenna array biosensor. (a) EBOV sGP sandwich assay format. (b) Calibration curve of sGP tested on the nanoantenna array using LUMP method

(N=27, error bars stand for standard deviations). (d) Calibration curve of sGP tested on the nanoantenna array using PIX method at low antigen concentrations (N=27, error bars stand for standard deviations). (e) and (f) Bar graph and scatter point plots of fluorescence intensity distributions of positive and negative samples in EBOV sGP test at 1:5000 antigen dilution in human plasma. (N=24 for true positive samples, and N=12 from true negative samples. Data is collected from independent devices.)

Figure 4a shows the assay format of EBOV sGP-spiked human plasma test using the nanoantenna array, which is similar to EBOVgp-Fc test (Figure 3a) except for the substitution of EBOVgp-Fc with sGP. The nanoantenna array biosensor demonstrated large dynamic response to EBOV sGP dilution from 1:10,000 to 1:10 in human plasma using the LUMP method (Figure 4b). The measurement results fit well with the well-established five-parameter logistic curve fitting. The LoD of sGP in human plasma was determined to be 10.7 pg/mL (1: 12,000 dilution) by five-parameter logistic curve fitting and consideration of three-time standard deviation of background signal using the LUMP method. In comparison, the conventional ELISA of the same sample only detected sGP at a 1: 128 dilutions, which is about 1 ng/mL (**Figure S2** in **ESI**).

The sensor surfaces were then further characterized using PIX method aiming at extending the EBOV sGP detection limit to even lower concentration. Figure 4c shows a sample imaging analysis of the nanoantenna array chip after assay using PIX method highlighting the fluorescence "hotspots" on the sensor surface. Analysis of the EBOG sGP spiked samples using PIX method showed a linear correlation between the fluorescence hotspot numbers on-chip and the concentrations of EBOV-sGP antigen (Figure 4d) from 1:32,000 dilutions (~4 pg/mL) to 1: 1,000,000 dilutions (~128 fg/mL) with the R^2 value of 0.99, indicating excellent dynamic responses. The PIX signal showed slight saturation for the antigen concentrations higher than 1:32,000 but is still distinguishable using the 5 parameter logistic (5PL) model[15]. This is a result of the combination of increased background signal level and gradual loss of hotspot flickering

behaviors at high concentration. In the LUMP mode, the sensor demonstrated promising dynamic responses from 1:10 dilutions to 1:1000 dilutions with the R^2 value of 0.95. The error bars represent standard deviations of 27 independent data points, and the variation is a combination of nonspecific binding in the matrices. Combining with the results from LUMP method at higher antigen concentrations and PIX method at low antigen concentration, the nanoantenna-based assay has achieved over five orders of magnitudes of dynamic response against EBOV antigen with the detection limit of 1: 588,000 dilutions (~220 fg/mL). This is a significant improvement in detection limit compared to the existing FDA-recommended EBOV rapid immunoassay test (~240,000 folds) and EBOV immunoassay sensors in the research phase (~4500 folds).

The mock clinical evaluation of the nanoantenna array EBOV sGP test performed using LUMP method on human plasma samples spiked with EBOV sGP at 2X LoD (1:5,000 dilution). The blind EBOV sGP test utilized 24 true positive samples and 12 true negative samples. The fluorescence intensity from the positive and negative samples were plotted in Figure 4e and 5f as bar graph and scatter point plot, respectively. ANOVA test revealed that the fluorescence intensities from positive sample group are significantly different from the negative ones with the p value of 0.0007, F value of 13.3 (Figure 4e). In the sGP-spiked positive samples, the fluorescence intensity is averaged at around 300. And, the negative control samples showed the average fluorescence intensity level of 220. The threshold is set at 230 to achieve a lower than 5% false positive sample rate statistically while maintaining a relatively high specificity (low false negative rate). The diagnostic sensitivity of the nanoantenna array-based immunoassay for detecting EBOV sGP-spiked human plasma reached 95.8% (efficacy to detect true positive), and the selectivity reached 91.7% (efficacy to determine true negative) (Figure 4f). The high diagnostic sensitivity has proved that the feasibility of the nanoantenna array-based EBOV sensor in effective screening

of EBOV sGP positive samples in human plasma. We utilized a 20-day evaluation method to characterize our assay precision and repeatability[16]. The assay was performed by spiking EBOV sGP at 1:5000 to human plasma samples from one donor, and repeated for 20 consecutive days with 3 replicas per day. The results demonstrated that the coefficient of variation (CV) of 20-day repeatability test is 3.20%, in-lab precision (variation) is 8.12%. The detailed precision and repeatability analysis is included in **ESI**. This has validated the repeatability of the nanoantenna test, and demonstrated its overall analytical stability.

The nanoantenna-based ultrasensitive EBOV antigen sensor has elevated the sensitivity compared to existing immunoassay tests tremendously. This entitles the immunoassay-based sensor with more accurate diagnostic values in EBOV disease control and screening, which can potentially be used in field tests. This work developed an orthogonal diagnostic method with improved sensitivity to current immunoassay that could be used as an alternative or a confirmatory assay to PCR diagnostics. With the successful ultra-sensitive detection of EBOV antigens, we anticipate future development of this nanoantenna-based sensor as a more universal biosensing platform to provide early detection options to a wider range of pathogens that can cause severe illness.

Experimental Sections:

Nanoantenna nanofabrication:

The nanoantenna array biosensor was fabricated through NIL and thin-film processes. NIL was first performed on a silicon dioxide substrate with 150nm-thick nanoimprint resist (NXR-1025, Nanonex Corporation). The patterned resist layer was dry-etched under reactive ion etching (50W,

5mTorr, 10 sccm O_2, 1.5 minutes), exposing the nano-disk feature on SiO_2 layer. The subsequent Cr coating, lift-off process, and plasma etching of SiO_2 created SiO_2 pillar arrays on the substrate with 52 nm – 61 nm in height and 100 nm in diameter. In the final step, evaporation of Ti/Au (15Å/510Å) formed the top gold metal disks and bottom backplane structures.

Nanoantenna surface functionalization:

Before any bioassays, the nanoantenna sensor surfaces were treated with 3,3'-dithiobis (sulfosuccinimidyl propionate) (DTSSP, Thermo Fisher) for 18 hours to create thiol-NHS self-assembled monolayer (SAM) as biomolecule binding anchors. After SAM layer overnight assembly, 10 μg/mL of protein A/G in 1X PBS buffer was added on the sensor surface and incubated at room temperature for 2 hours.

Antibody direct assay and fluorescence enhancement characterization:

The sensor surfaces were treated with 3,3'-dithiobis (sulfosuccinimidyl propionate) (DTSSP, Thermo Fisher) for 18 hours to create thiol-NHS self-assembled monolayer (SAM) as biomolecule binding anchors. After SAM layer overnight assembly, 10 μg/mL of protein A/G in 1X PBS buffer was added on the sensor surface and incubated at room temperature for 2 hours. The target molecules – goat anti-human IgG with IRDye-800cw labels – at various concentration in 1X PBS (0.2 μg/mL, 1 μg/mL and 5 μg/mL) bound specifically to protein A/G on the sensor surface in 2 hours. All sensor surfaces were cleaned using 0.5% Tween 20 in 1X PBS buffer after each assay step. Before imaging, the sensors were washed three times additionally using distill water to eliminate salt residues on the sensor. We also performed the same assay protocol on flat gold and

SiO_2 surface as control experiments. SEM imaging has been used to inspect the sensor surfaces after assay.

Here, we define fluorescence enhancement factor (EF) as ratio of fluorescence intensity at 800 nm from the nanoantenna array surface over that from a conventional flat substrate under the same assay condition:

$$EF = I_{nanoantenna\ array@800nm} / I_{Au@800nm} \quad (1)$$

Where $I_{nanoantenna\ array@800nm}$ is the fluorescence intensity at 800nm from the nanoantenna array sensor surface after the assay, and $I_{Au@800nm}$ is the fluorescence intensity at 800nm from flat gold substrate.

Nanoantenna array EBOV sandwich assay:

The sensor was first immobilized with a DTSSP SAM layer in an overnight process followed by protein A/G surface treatment for 2 hours at room temperature. After Protein A/G coating, the cAb (rabbit anti-EBOV-GP polymonoclonal capture antibodies) at 10 μg/mL was bound to the surface of the nanoantenna array by incubating 2 hours at room temperature. Non-specific binding sites on the sensor were blocked using 1X PBS buffer with 4% BSA overnight at 4°C. Different concentrations of the antigen, EBOVgp-Fc, in 4% BSA was bound to the capture antibody for 2 hours at room temperature. The bound EBOVgp-Fc was detected using 1 μg/mL dAb (mouse anti-EBOV GP monoclonal detection antibody), which was stained with 0.2 μg/mL of IRDye800cw-labeled goat anti-mouse IgG secondary antibody. Between each assay step, the sensor surfaces were washed three times with 1X PBS buffer with 0.5% Tween 20 detergent. This assay protocol was optimized for the best the nanoantenna array-based sandwich immunoassay results (see

capture and detection antibody optimization in **Table S1** the **ESI**). We performed side-by-side comparison between our proposed the nanoantenna array-based sandwich assay and ELISA using the same antibodies and antigens. In the ELISA, HRP and TMB substrate-enzyme system was used instead of the IRDye800cw-labeled secondary antibody used in the nanoantenna array plate. All the other ELISA conditions (antibodies and antigen concentrations, incubation times and temperatures, and washing steps) were kept identical to the nanoantenna array EBOV assay in the protocol. The cAb-dAb pair of antibodies did not react with the glycoprotein of Sudan virus (SUDV), a filovirus belonging to the same genus than EBOV (Ebola virus), and Marburg virus (MARV), a filovirus that belongs to a different genus (Marburg virus), indicating that the assay was specific for EBOV. Furthermore, omission of any of the components of the antigen-antibody sandwich resulted in minimal background-level signal in both the nanoantenna array and ELISA formats of the test.

Lumpsum and Pixelated on-chip fluorescence detection methods:

During fluorescence microscopy testing, we utilize excitation laser at 785 nm wavelength with the power intensity of 10 mW/cm^2 to illuminate the nanoantenna array sensor surface through 10X microscopy lens. The laser beam has gone through vibrating micromirrors at both X and Y directions, forming an active scanning area of 150 μm × 150 μm on-chip. The fluorescence intensity is analyzed in the range of 795nm-805nm using an Electron Multiplying CCD (EMCCD, Andor iXon, Oxford Instruments, UK). Two imaging methods, Lumpsum (LUMP) and Pixelated (PIX), have been developed to target at either high or low EBOV antigen concentrations. At high antigen concentrations, LUMP method utilizes the overall fluorescence intensity on the sensor surface to correlate it with the antigen concentration in assay. At low antigen concentrations, PIX

method introduces imaging processing to count individual fluorophores glowing events (hotspot flickering) using an EMCCD (Figure 1d). The PIX algorithm counts localized maxima and monitor the maxima changes (fluorophore flickering) over 100 frames (with the total time period of 10s). As fluorophore light emission is enhanced by the nanoantenna array platform, and even weak light emission from discretely distributed fluorophores can be visualized using PIX as hotspots in a microscopy image (20X objective lens). The PIX method significantly improves the limit of detection (LoD) of the nanoantenna array-based EBOV assay.

Author Information

S.Y.C. originated the idea of use of the nanoantenna array structures for immunoassay fluorescence and detection sensitivity enhancement and designed and directed the research. S.Y.C. and G.K made initial experimental planning. F.Z and Z.S designed and performed the experiments of immunoassay and optical characterization. F.Z, L.Z, G.C. and S.Y.C. designed immunoassay protocol. K.K. and G.K. developed and purified the Ebola virus antigens and antibodies. F.Z., Z.S. and S.Y.C designed and fabricated the nanoantenna array samples. F.Z., Z.S., G.K, and S.Y.C. contributed to data analysis and manuscript writing.

Acknowledgement

The work was supported by a grant from the Bill and Melinda Gates Foundation (OPP1117592) to S.Y.C. and G.K., the Defense Threat Reduction Agency (HDTRA1-16-C-0025) to S.Y.C. and G.K., and National Science Foundation Scalable Nanomanufacturing Program (CMMI-1635443) to S.Y.C. The work was also supported by intramural funding from the Food and Drug Administration to G.K. The authors acknowledge the use of Princeton's Imaging and Analysis

Center, which is partially supported by the Princeton Center for Complex Materials, a National Science Foundation (NSF)-MRSEC program (DMR-1420541).

Our contributions are an informal communication and represent our own best judgment. These comments do not bind or obligate FDA.

Competing Interests

The authors declare no competing financial interests.

Electronic Supporting Information

Supporting information is available online. It includes fluorescence hotspots imaging using PIX method, antibody pair optimization, EBOV assay precision and repeatability tests, Fc section non-specific binding evaluation, proteins translated from the EBOV GP gene produced during infection, and monoclonal anti-EBOV GP antibody specificity test using ELISA.

REFERENCES

[1] a) S. Baize, D. Pannetier, L. Oestereich, T. Rieger, L. Koivogui, N. Magassouba, B. Soropogui, M. S. Sow, S. Keita, H. De Clerck, A. Tiffany, G. Dominguez, M. Loua, A. Traore, M. Kolie, E. R. Malano, E. Heleze, A. Bocquin, S. Mely, H. Raoul, V. Caro, D. Cadar, M. Gabriel, M. Pahlmann, D. Tappe, J. Schmidt-Chanasit, B. Impouma, A. K. Diallo, P. Formenty, M. Van Herp, S. Gunther, *N Engl J Med* **2014**, *371*, 1418; b) D. Gatherer, *J Gen Virol* **2014**, *95*, 1619.

[2] a) W. E. R. Team, *New England Journal of Medicine* **2014**, *371*, 1481; b) A. Kaushik, S. Tiwari, R. D. Jayant, A. Marty, M. Nair, *Biosensors and Bioelectronics* **2016**, *75*, 254; c) P. Nouvellet, T. Garske, H. L. Mills, G. Nedjati-Gilani, W. Hinsley, I. M. Blake, M. D. Van Kerkhove, A. Cori, I. Dorigatti, T. Jombart, *Nature* **2015**, *528*, S109.

[3] a) C. Drosten, S. Gottig, S. Schilling, M. Asper, M. Panning, H. Schmitz, S. Gunther, *J Clin Microbiol* **2002**, *40*, 2323; b) J. S. Towner, P. E. Rollin, D. G. Bausch, A. Sanchez, S. M. Crary, M. Vincent, W. F. Lee, C. F. Spiropoulou, T. G. Ksiazek, M. Lukwiya, F. Kaducu, R. Downing, S. T. Nichol, *J Virol* **2004**, *78*, 4330; c) T. M. Uyeki, A. K. Mehta, R. T. Davey, Jr., A. M. Liddell, T. Wolf, P. Vetter, S. Schmiedel, T. Grunewald, M. Jacobs, J. R. Arribas, L. Evans, A. L. Hewlett, A. B. Brantsaeter, G. Ippolito, C. Rapp, A. I. Hoepelman, J. Gutman, U. S. E. C. N. o. C. M. o. E. V. D. P. i. t. U. S. Working Group of the, Europe, *N Engl J Med* **2016**, *374*, 636; d) A. Grolla, A. Lucht, D. Dick, J. E. Strong, H. Feldmann, *Bull Soc Pathol Exot* **2005**, *98*, 205.

[4] a) A. Borst, A. Box, A. Fluit, *European journal of clinical microbiology and infectious diseases* **2004**, *23*, 289; b) B. C. Millar, J. Xu, J. E. Moore, *Journal of clinical microbiology* **2002**, *40*, 1575; c) E. M. Leroy, S. Baize, C. Y. Lu, J. B. McCormick, A. J. Georges, M. C. Georges-Courbot, J. Lansoud-Soukate, S. P. Fisher-Hoch, *J Med Virol* **2000**, *60*, 463.

[5] P. Brangel, A. Sobarzo, C. Parolo, B. S. Miller, P. D. Howes, S. Gelkop, J. J. Lutwama, J. M. Dye, R. A. McKendry, L. Lobel, M. M. Stevens, *ACS Nano* **2018**, *12*, 63.

[6] Y. Chen, R. Ren, H. Pu, X. Guo, J. Chang, G. Zhou, S. Mao, M. Kron, J. Chen, *Sci Rep* **2017**, *7*, 10974.

[7] a) M. I. Stockman, *Science* **2015**, *348*, 287; b) J.-J. Xu, W.-W. Zhao, S. Song, C. Fan, H.-Y. Chen, *Chemical Society Reviews* **2014**, *43*, 1601; c) F. Zang, K. Gerasopoulos, A. D. Brown, J. N. Culver, R. Ghodssi, *ACS Appl Mater Interfaces* **2017**, *9*, 8471; d) F. Zang, K. Gerasopoulos, X. Z. Fan, A. D. Brown, J. N. Culver, R. Ghodssi, *Chem Commun* **2014**, *50*, 12977; e) F. Zang, K. Gerasopoulos, X. Z. Fan, A. D. Brown, J. N. Culver, R. Ghodssi, *Biosens Bioelectron* **2016**, *81*, 401.

[8] a) A. G. Brolo, *Nat Photonics* **2012**, *6*, 709; b) M. D. Baaske, M. R. Foreman, F. Vollmer, *Nat Nanotechnol* **2014**, *9*, 933; c) P. M. Kosaka, V. Pini, J. J. Ruz, R. A. da Silva, M. U. Gonzalez, D. Ramos, M. Calleja, J. Tamayo, *Nat Nanotechnol* **2014**, *9*, 1047.

[9] a) A. Fratalocchi, C. M. Dodson, R. Zia, P. Genevet, E. Verhagen, H. Altug, V. J. Sorger, *Nat Nanotechnol* **2015**, *10*, 11; b) G. A. Lopez, M. C. Estevez, M. Soler, L. M. Lechuga, *Nanophotonics-Berlin* **2017**, *6*, 123.

[10] a) W.-D. Li, F. Ding, J. Hu, S. Y. Chou, *Optics express* **2011**, *19*, 3925; b) C. Wang, Q. Zhang, Y. Song, S. Y. Chou, *ACS nano* **2014**, *8*, 2618; c) L. Zhou, F. Ding, H. Chen, W. Ding, W. Zhang, S. Y. Chou, *Analytical chemistry* **2012**, *84*, 4489.

[11] K. Konduru, S. B. Bradfute, J. Jacques, M. Manangeeswaran, S. Nakamura, S. Morshed, S. C. Wood, S. Bavari, G. G. Kaplan, *Vaccine* **2011**, *29*, 2968.

[12] W. Ou, J. Delisle, K. Konduru, S. Bradfute, S. R. Radoshitzky, C. Retterer, K. Kota, S. Bavari, J. H. Kuhn, P. B. Jahrling, G. Kaplan, C. A. Wilson, *J Virol Methods* **2011**, *174*, 99.

[13] A. Kinkhabwala, Z. F. Yu, S. H. Fan, Y. Avlasevich, K. Mullen, W. E. Moerner, *Nat Photonics* **2009**, *3*, 654.

[14] I. G. Theodorou, Q. F. Jiang, L. Malms, X. Y. Xie, R. C. Coombes, E. O. Aboagye, A. E. Porter, M. P. Ryan, F. Xie, *Nanoscale* **2018**, *10*, 15854.

[15] P. G. Gottschalk, J. R. Dunn, *Anal Biochem* **2005**, *343*, 54.

[16] D. Chesher, *Clin Biochem Rev* **2008**, *29 Suppl 1*, S23.

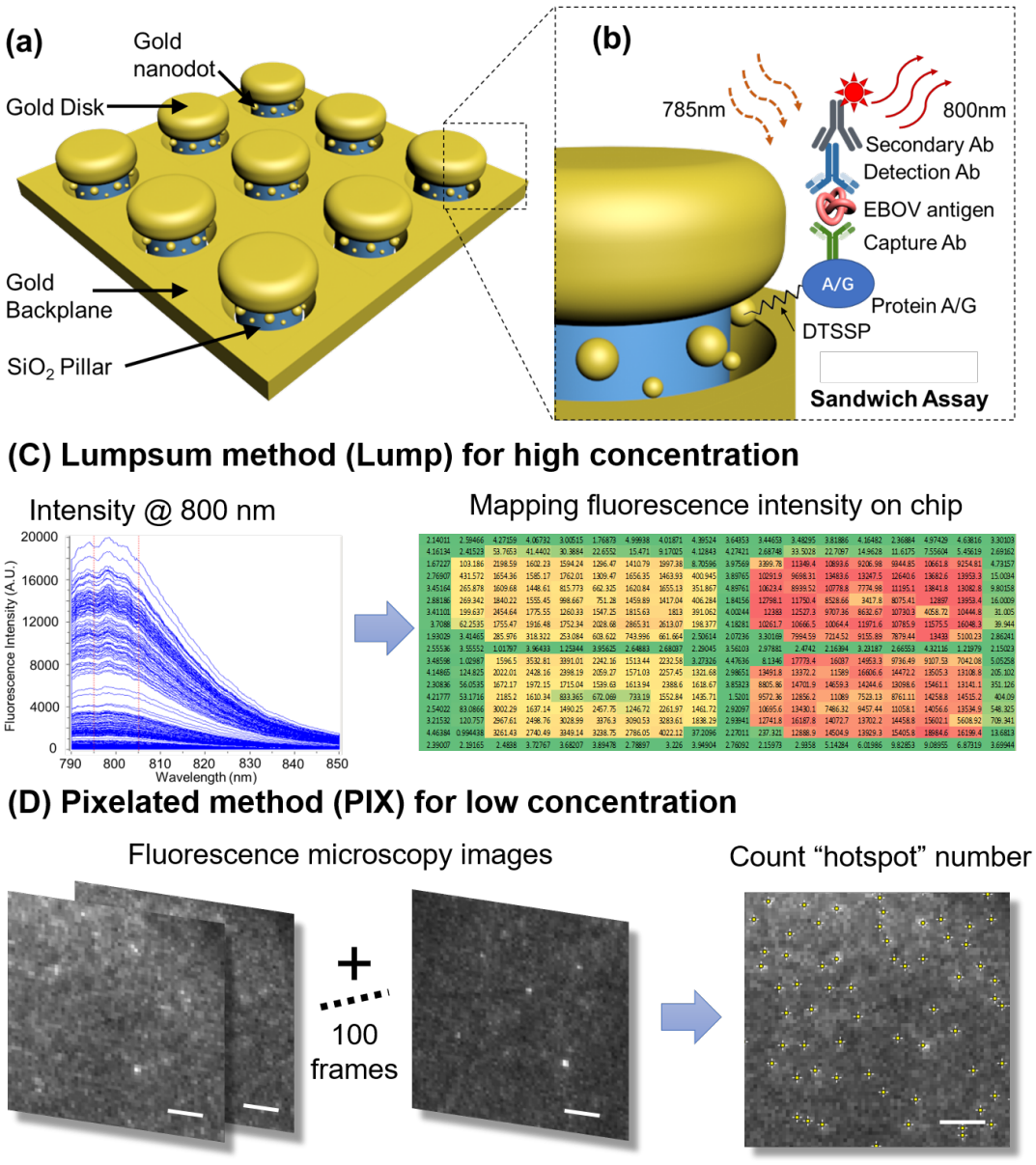

Figure 1. The EBOV sensor nanostructures and fluorescence sensing methods. (a) Schematic of nanoantenna array. (b) Exploded view showing the details of single nanopillar structures and a sample EBOV sandwich assay structure on-chip. (c) Lumpsum (LUMP) method for counting overall fluorescence intensity at high antigen concentration. (d) Pixelated (PIX) method for low antigen concentration analysis by fluorescence hotspot counting (scale bars represent 10µm).

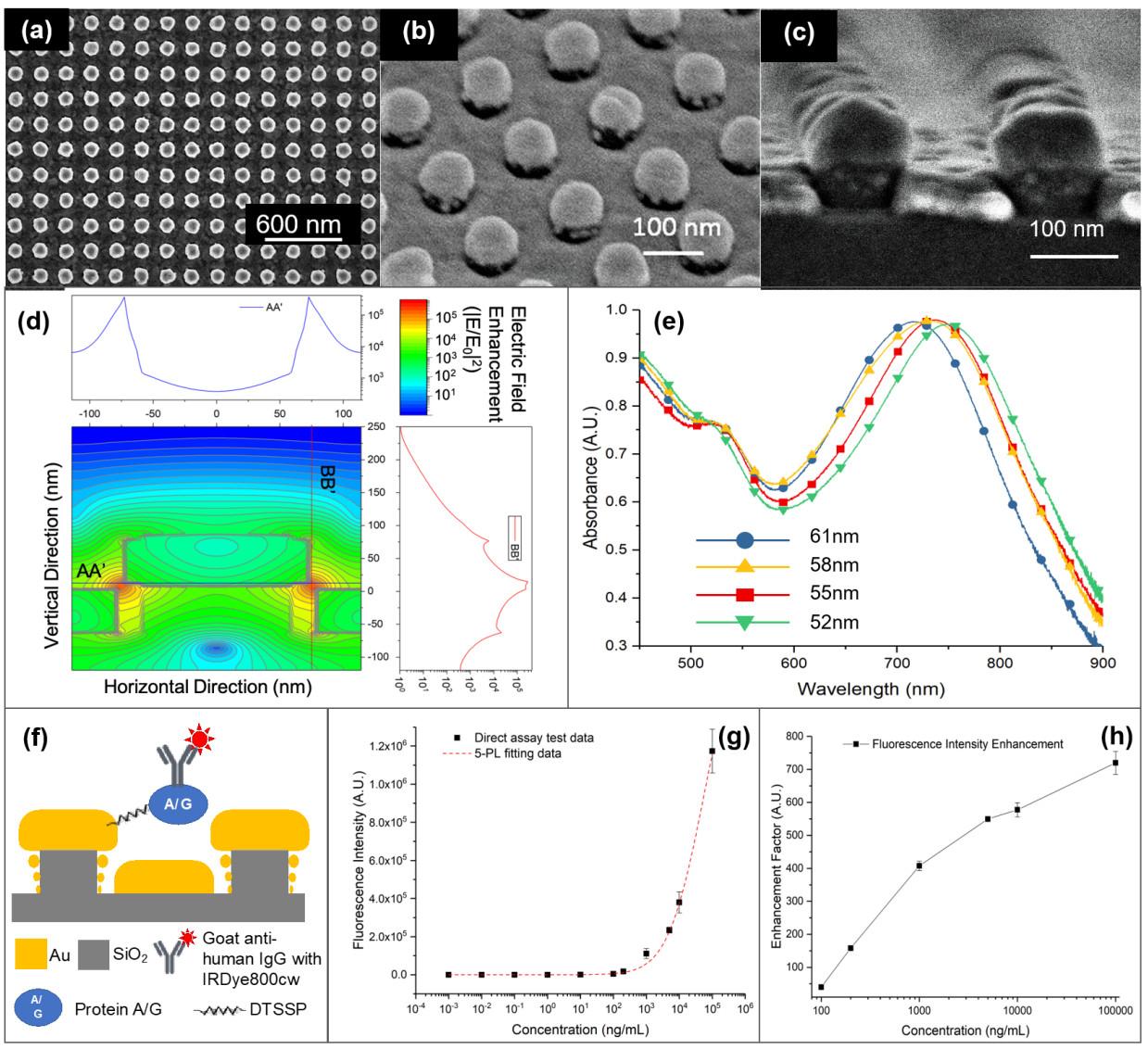

Figure 2. Characterization of the nanoantenna array EBOV sensor after nanofabrication. (a) Scanning electron microscopy (SEM) image showing the top-down view of the nanoantenna array after nanofabrication processes on a 4-inch wafer; (b) a prospect view SEM image showing the Au nano disks on SiO_2 pillars; (c) SEM image showing discrete distribution of gold nanoparticles on the nanoantenna array SiO_2 nanopillar sidewalls. (d) FDTD simulation of the electrical field enhancement ($|E/E_0|^2$) in a nanoantenna unit. (e) Absorption spectra of the nanoantenna array with different nanopillar heights (52nm – 61nm). (f) Schematic of antibody direct binding assay on the nanoantenna array biosensor. (g) Antibody direct binding assay standard curve. (i) Fluorescence intensity enhancement on the nanoantenna array compared to flat gold surfaces after antibody binding assay. (N=27, error bars stand for standard deviations)

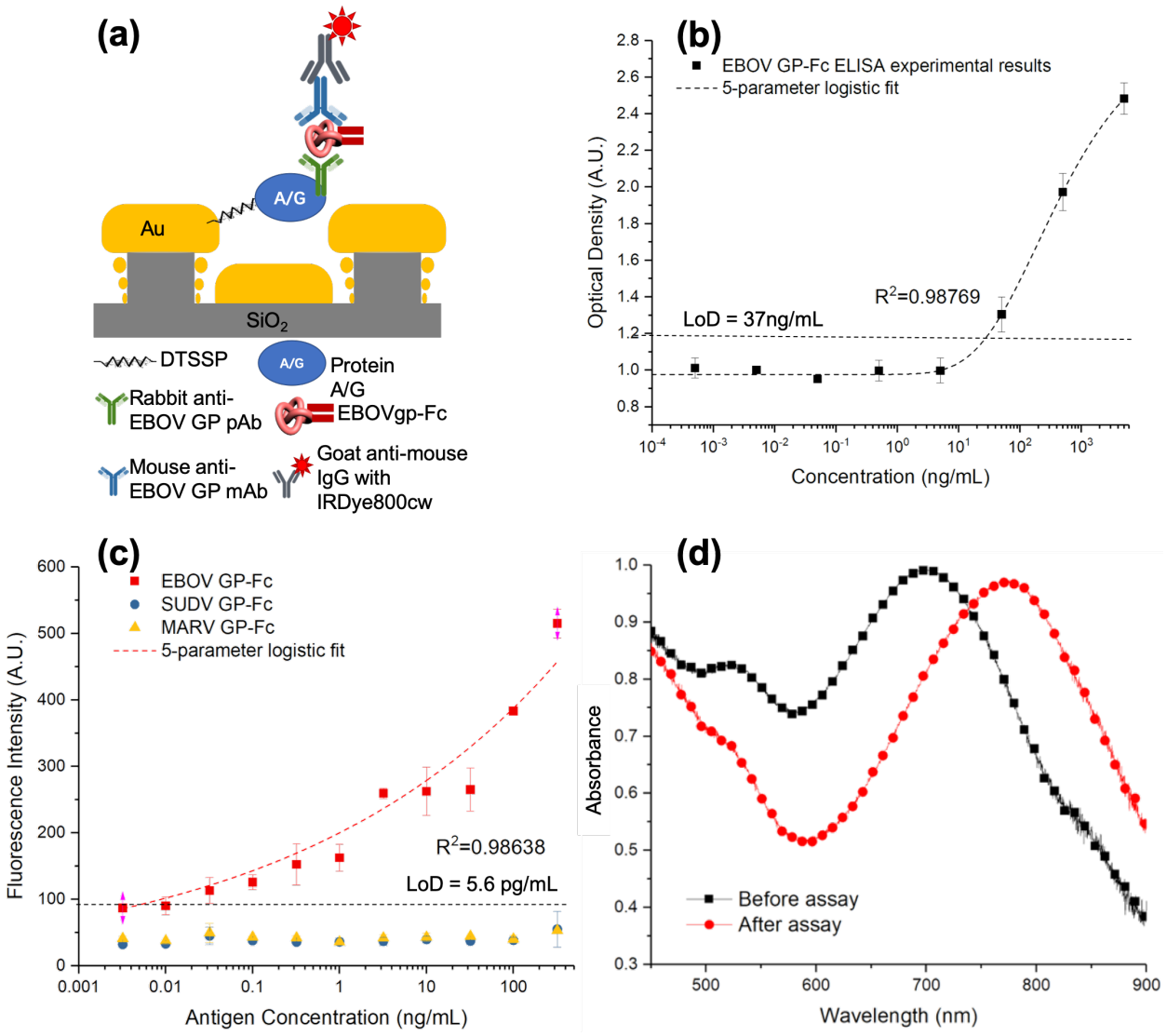

Figure 3. EBOVgp-Fc-spiked PBS buffer bioassay test. (a) Sandwich assay format for EBOVgp-Fc detection using the nanoantenna array biosensor. (b) Bioassay responses to increasing EBOVgp-Fc antigen concentration in ELISA. (N=27, error bars stand for standard deviations) (c) Sandwich assay responses to increasing EBOVgp-Fc antigen concentration using the nanoantenna array. (N=27, error bars stand for standard deviations) (d) the nanoantenna array absorbance characteristics change before and after sandwich assay against EBOVgp-Fc at 320 ng/mL.

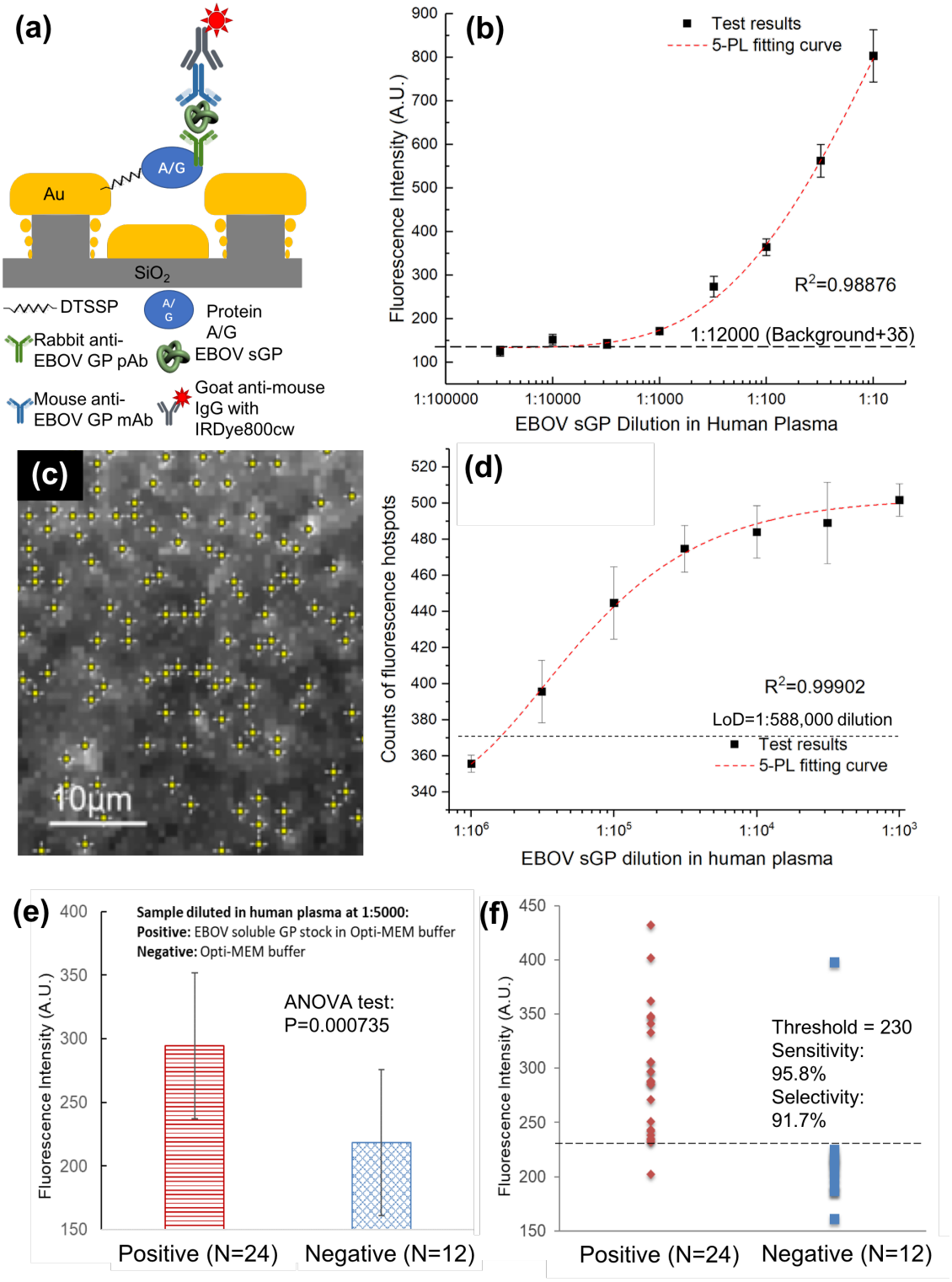

Figure 4. EBOV sGP-spiked human plasma study using the nanoantenna array biosensor. (a) EBOV sGP sandwich assay format. (b) Calibration curve of sGP tested on the nanoantenna array using LUMP method

(N=27, error bars stand for standard deviations). (d) Calibration curve of sGP tested on the nanoantenna array using PIX method at low antigen concentrations (N=27, error bars stand for standard deviations). (e) and (f) Bar graph and scatter point plots of fluorescence intensity distributions of positive and negative samples in EBOV sGP test at 1:5000 antigen dilution in human plasma. (N=24 for true positive samples, and N=12 from true negative samples. Data is collected from independent devices.)

Table of Contents (ToC):

Title: Ultra-sensitive Ebola antigen sensing via three-dimensional nanoantenna arrays

Keywords: nanoantenna, optical resonance, fluorescence enhancement, biosensors, Ebola

Authors: Faheng Zang, Zhijuan Su, Liangcheng Zhou, Krishnamurthy Konduru, Gerardo Kaplan and Stephen Y. Chou*

Abstract: A nanoantenna-array biosensor is developed for ultrasensitive Ebola virus antigens detection. This nanostructured sensor manufactured via nanoimprint lithography shows superior diagnostic capability against Ebola soluble glycoprotein with 240,000-fold better sensitivity than the existing rapid Ebola assays. It highlighted the nanoantenna sensor's tremendous potential as a universal next-generation bioassay platform for significant fluorescence enhancement, bioassays compatibility, low cost, and scalable manufacturing.

ToC figure: